Measurement: Sensors 42 (2025) 101973

Contents lists available at ScienceDirect

Measurement: Sensors

journal homepage: www.sciencedirect.com/journal/measurement-sensors

A novel approach for measuring dielectric properties of materials using multi-length bifilar technique

Iman Farhat [a,*], Raffaele Persico [b], Justin Stellini [a], Andrea Cataldo [c], Julian Bonello [a], Lourdes Farrugia [a]

[a] Department of Physics, University of Malta, Triq Ta Qorqq, Msida, MSD2080, Malta
[b] Department of Engineering of the Environment and the Territory DIAM, University of Calabria, Via P. Bucci, Cubo 45 A, Calabria, 87036 Rende, Italy
[c] Department of Engineering for Innovation, Ecotekne - Palace O - Provincial road Lecce-Monteroni, Lecce, 73100 LECCE (LE), Italy

A R T I C L E I N F O

Keywords:
Bifilar transmission line
Dielectric properties
Complex permittivity
Loss tangent
Material characterisation
Liquids
Soil

A B S T R A C T

A novel methodology is introduced for measuring the dielectric properties of materials using a bifilar transmission line for material characterisation. The investigation targets liquids and semi-solid media, including gels, pastes, and moist soils, with dielectric properties measured across the frequency range of 0.3 to 1.5 GHz. Conventional dielectric measurement methods often face limitations when dealing with heterogeneous or high-loss materials, such as soil, biological tissues, and various liquid compositions. Leveraging a dual-rod configuration, the proposed bifilar line enables a precise dielectric assessment by optimising the interaction between the sample and the measurement field. Experimental results demonstrate the technique's efficacy in capturing key dielectric parameters, including permittivity and loss tangent. The findings suggest that this approach not only enhances measurement accuracy for complex materials but also offers potential for in-situ and real-time applications in environmental monitoring, agriculture, and material science.

1. Introduction

Reflectometry measurements remain a fundamental technique for measuring electromagnetic parameters of materials under test (MUT) in the radio and microwave frequency ranges. Its importance comes from its accuracy, cost effectiveness and suitability for continuous real-time measurements with remote control capabilities [1,2]. A primary application of interest is the dielectric characterisation of materials, particularly in agricultural applications for soil moisture monitoring [3,4]. This method has demonstrated versatility in detecting organic pollutants in sandy soil as well as to be characterising soil dielectric properties [1,5]. Furthermore, it has proven valuable in food quality assessment, enabling water content measurements in various agricultural products including oils, soybeans, coffee, bran, and corn [6–8].

This research focuses specifically on frequency domain reflectometry (FDR) applications for the dielectric characterisation of liquids and soil in the microwave range. Although TDR instrumentation typically offers cost advantages, the FDR approach enables the implementation of rigorous calibration procedures, thereby enhancing the accuracy of material dielectric property measurements [9,10]. Throughout this paper, we use "semi-solid" to denote materials that are neither rigid solids nor freely flowing liquids, and that present quasi-homogeneous dielectric behaviour over the probe's sensing volume. This category includes gels, pastes, and moist soils.

Beccaro et al. (2016) simulated and tested various probe designs — including bifilar, coaxial, microstrip, and helical — for detecting ethanol adulteration in fuel using the TDR technique. Although all four probes enabled the detection of ethanol adulterated with water, the helical probe performed best. The bifilar design served as a baseline prototype for comparative analysis [11]. In the context of industrial applications, a commercial TDR bifilar probe was used in conjunction with an open-ended coaxial probe in the FDR to assess the dielectric properties of milling grist. Knowing these properties helped in designing bifilar electrostatic filters for purifying air in food processing environments [12]. Persico and Pieraccini (2018) developed a frequency-domain theory that demonstrates, in principle, how a TDR probe can separate a material's permittivity and permeability from its complex response [10]. They examined the identifiability and retrieval conditions for these inversions. Subsequent studies progressed from initial numerical validations to a multi-length approach that retrieves the dispersion law, $\varepsilon(f)$, without imposing a parametric model [13]. This was followed by a bifilar proof-of-concept by Cataldo et al. (2022) [14]. Cataldo et al. presented a microwave FDR system utilising a customised bifilar probe alongside a miniaturised vector network analyser

* Corresponding author.
E-mail address: iman.farhat@um.edu.mt (I. Farhat).

https://doi.org/10.1016/j.measen.2025.101973
Received 18 June 2025; Received in revised form 16 September 2025; Accepted 3 October 2025
Available online 16 October 2025

(m-VNA). This setup enabled the extraction of single-pole Debye parameters (the real part of the complex relative permittivity at static and infinite frequency, relaxation time, and conductivity) from soil samples, highlighting its potential for low-cost, in-field sensing The present work extends this methodological progression by providing experimental validation and recovery of Debye parameters.

The proposed methodology integrates theoretical analysis of bifilar transmission lines with detailed numerical electromagnetic simulations based on a finite-difference time-domain (FDTD) model implemented in CST Studio Suite [15]. In contrast to previous research that validated models using a single transmission line probe length, this study systematically investigates materials using a bifilar probe with multiple lengths. This approach enables the characterisation of regions at different depths within a (MUT), such as soil, where the transmission line model yields acceptable accuracy, thereby supporting reliable measurement of soil moisture at various levels. Such depth-resolved measurement techniques could also benefit pollution detection and the identification of soil contamination at different levels [16].

The subsequent sections present the theoretical framework, followed by extensive numerical validation and experimental results. The findings advance both the theoretical understanding of the bifilar probe and provide practical guidelines for probe design and measurement interpretation across an expanded range of material properties [17, 18]. This comprehensive approach bridges the gap between theoretical modelling and practical applications in field conditions [19].

2. Conversion model

2.1. Mathematical model

The focus here is on the bifilar probes in the frequency domain, modelled as a transmission line consisting of two long, perfect electric conductors parallel to each other Fig. 1. The characteristic impedance of the bifilar depends on its geometry and the permittivity of the medium. For a bifilar line consisting of two parallel cylindrical conductors with the same radius r, separation d, and surrounded by a medium with permittivity ε_r, the characteristic impedance is [20,21]:

$$Z_l = \frac{120\pi}{\sqrt{\varepsilon_r}} \cosh^{-1}(\frac{d}{2r}) \tag{1}$$

The transmission line consists of two sections: the first is a segment with intrinsic impedance Z_g (i.e., the generator's characteristic impedance), which is matched to the generator and remains in the air. This air-exposed section is connected to the second part: conductive rods that are inserted into the MUT, as illustrated in Fig. 1.

The input impedance of the line at the abscissa of the air-MUT interface looking towards the load is given by [22]

$$Z(-L) = Z_l \frac{Z_L + jZ_l \tanh(\gamma L)}{Z_l + jZ_L \tanh(\gamma L)} \tag{2}$$

where γ is the propagation constant for a transmission line defined as

$$\begin{aligned}\gamma &= j\omega\sqrt{\mu_0\varepsilon_0\varepsilon_r} \\ &= j\frac{2\pi f}{c_0}\sqrt{\varepsilon_r}\end{aligned} \tag{3}$$

The proposed bifilar probe terminates in an open-ended transmission line; the load represents an open circuit with infinite impedance, preventing any current flow regardless of the applied voltage. The input impedance at the given abscissa (air/MUT interface) is therefore determined by this boundary condition ($Z_L \Longrightarrow \infty$). In this quest, it is simplified to a high impedance $Z_L = 10^6\ \Omega$ for an open termination, and modified as needed, as explained in Section 3.1.

Since direct impedance measurements along the transmission line are challenging, the problem is reformulated using the reflection coefficient, which can be measured more readily. This reflection coefficient Γ is evaluated at the air-MUT interface from the air side and is defined as.

$$\Gamma(-L) = \frac{Z(-L) - Z_g}{Z(-L) + Z_g} \tag{4}$$

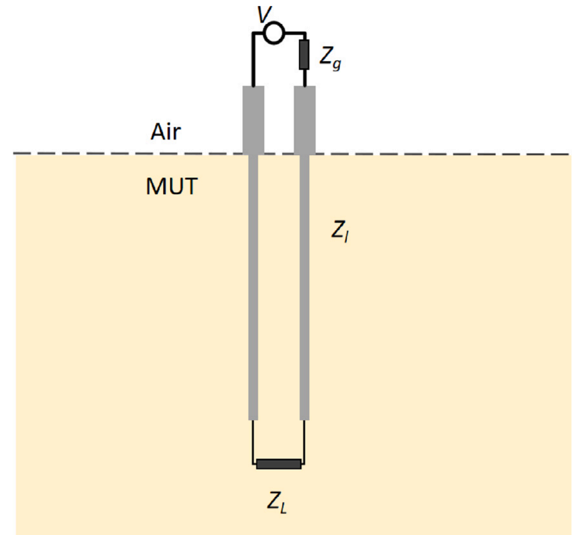

Fig. 1. Scheme for a finite transmission line applicable to a TDR probe immersed in the medium to be investigated [1].

The input impedance model defined in Eq. (2) (substituting Eq. (1) and (3) into Eq. (4)) is then used to calculate the modelled reflection coefficient.

To retrieve the permittivity, a two-step algorithm implemented in MATLAB [23] is employed to minimise the residual between the measured and modelled reflection coefficients across all probe lengths. In this case, a multi-length cost function $\mathrm{F}(\theta, f)$ is adopted at a fixed frequency following the assumption proposed in [10]. The method relies on length diversity by sampling the one-port response at several physical probe lengths L_k over a narrow frequency window around a resonance. At fixed material properties, changing L alters the phase advance γL and shifts the resonance pattern; stacking $\Gamma(f, L_k)$ across lengths therefore provides independent constraints on the unknown permittivity. This renders the inversion better posed than using a single length. This aspect mathematically replaces frequency diversity with diversity in probe length. For each length L_k, we retrieve the Debye parameters $\theta = \{\varepsilon_l, \varepsilon_h, \tau, \sigma\}$ by minimising a frequency-domain misfit.

$$\mathrm{F}(\theta) = \sum_{k=1}^{M} \left| \Gamma_{(\mathrm{m/s})}(f, L_k) \ - \ \Gamma_{\mathrm{mod}}(f, \theta; L_k) \right|^2, \tag{5}$$

where $\Gamma_{(\mathrm{m/s})}$ is the actual reflection coefficient (measured/simulated) and the reflection coefficient $\Gamma_{\mathrm{mod}}(\theta; L_k)$ calculated by the model at the same probe length.

For a non-magnetic material, this optimisation yields a set of candidate solutions θ_k with corresponding minima $F_k^{\min}$. The optimal single-length estimate is denoted as $\theta^*_{k^*}$, where $k^* = \arg\min_k F_k^{\min}$. This implementation utilises the reflection coefficient Γ, also referred to as the $S11$ scattering parameter, in the characterisation of microwave one-port devices using a VNA.

The MUT complex permittivity $\varepsilon_r(f)$ has been determined through the Debye and Maxwellian model at each frequency and length using Eq. (6).

$$\varepsilon_r(f) = \varepsilon_l + \frac{\varepsilon_h - \varepsilon_l}{1 + j2\pi f\tau} - \frac{j\sigma}{2\pi f \varepsilon_0} \tag{6}$$

where ε_l is the relative permittivity at very low frequency, ε_h is the relative permittivity at very high frequency, σ is the electric conductivity, τ is the relaxation time. $\varepsilon_l, \varepsilon_h$, and τ are three positive parameters independent of the frequency; the first two are dimensionless, and the third one has the dimension of time. So, in the end, the model is based on four real non-negative parameters.

Varying the length of the rods results in sampling different effective sensing depths, as the standing-wave pattern and energy distribution depend on the rod length. Consistency of the retrieved parameters across these lengths, within the limits of measurement repeatability, serves as an intrinsic stability check for the MUT. If the parameters θ_k are consistent, the MUT can be considered homogeneous and stable throughout the probed volume. Conversely, significant variation among these parameters may indicate stratification, settling, trapped air, or temperature fluctuations.

2.2. Conversion algorithm

The algorithm employs a sophisticated two-step hybrid optimisation strategy that integrates the global exploration capabilities of a Genetic Algorithm (GA) with the local refinement precision of gradient-based optimisation. In the first step, the GA conducts a broad, randomised search across the defined boundaries of the Debye Dispersion law parameters. It generates a diverse set of potential solutions representing different combinations of Debye model parameters. The GA is configured with a population of 200 candidate solutions (randomised initial parameter sets) and a maximum of 100 generations. The selection of new generations is guided by a fitness evaluation based on a cost function, which leverages crossover and mutation mechanisms to explore promising regions of the parameter space. Once the GA identifies a promising region, the second step refines the solution using Sequential Quadratic Programming (SQP), a gradient-based optimisation method that acts as a local polishing process to fine-tune the parameters found by the GA. This hybrid approach is implemented using MATLAB's GA libraries, with the MATLAB syntax:

ga_options.HybridFcn = {@fmincon, hybrid_options},

where fmincon applies SQP for the local refinement phase.

The code is structured into five main sections: (1) the initial setup, where parameters and constants are defined; (2) data loading, which imports the reflection coefficient measurements; (3) GA configuration, where the algorithm parameters are set; (4) the core optimisation loop, which executes the inversion process; and (5) the final output section, which generates and visualises the results. The flux diagram describing the inversion algorithm is depicted in Fig. 2.

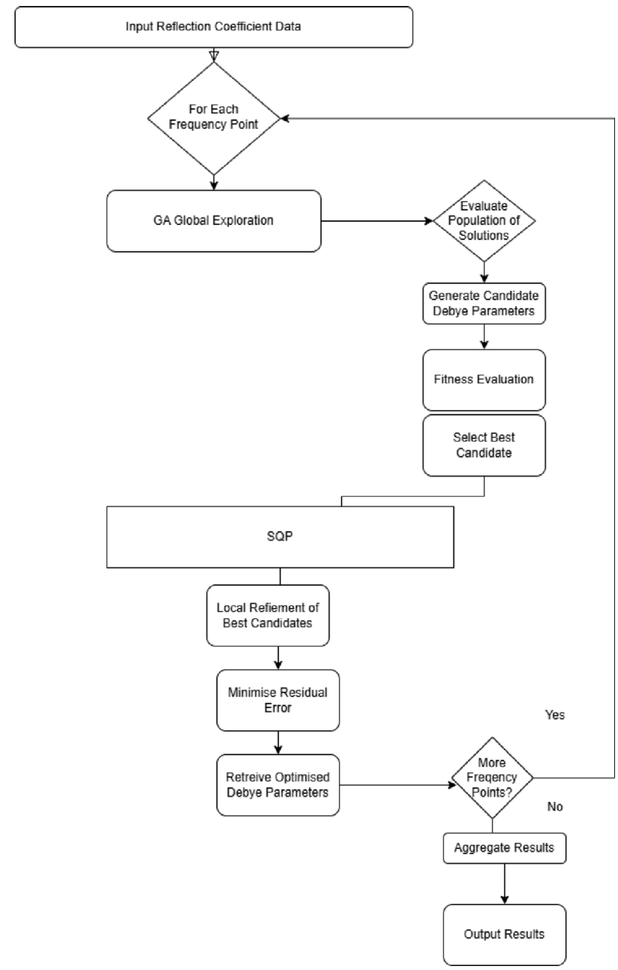

Fig. 2. The two-step hybrid GA flux diagram.

3. FDTD simulations and experimental validation

The developed bifilar probe is highly replicable, cost-effective, and customisable. It consists of two brass rods that can be adapted to suit various experimental needs. The two brass rods are connected to the probe head at the top with two banana connectors and connected to a VNA through a coaxial BNC transition. The schematic and line configuration of the bifilar probe is shown in Fig. 3. This bifilar line was previously investigated and discussed in [14]. However, the current proposed scheme is a multi-length bifilar system consisting of five bifilar lines of varying lengths: 14.17 cm, 15.70 cm, 17.20 cm, 18.60 cm, and 20.20 cm.

3.1. Connector–probe transition modelling and calibration

In the present workflow, the bifilar line including its connector–probe transition is explicitly modelled in CST Microwave Studio electromagnetic simulation software [15] and represented as a short section with parasitic capacitance and inductance at the rod junction. The bifilar CST finite-difference time domain (FDTD) model (Fig. 4b b) and its experimental setup in air are shown in Fig. 4(b) a. Furthermore, to ensure an accurate representation of real experimental conditions, a discrete 50 Ω port was embedded in the probe head. Its position in the connector–probe is also finely tuned, so that its performance matched that of its experimental setup in air. The transition parameters and the value for Z_L for an open termination are tuned using an air as a reference by measuring the reflection coefficient (S11) in air across the full frequency band. The model, including transition length and parasitic elements, are adjusted until the simulated air response aligns with the measured data within the acceptance band. This approach achieves functional equivalence to factory de-embedding implemented in commercial systems while providing transparent, user-controlled parameters.

The CST model of the bifilar line consists of two parallel cylindrical brass rods with the specifications considering centre-to-centre separation and the dimensions of the top head as illustrated in Fig. 1. Open boundary conditions were implemented using perfectly matched layers (PML) applied to the background material, which measured 10 mm in each direction. A computational mesh with a minimum element size of $\lambda/20$ at the highest operational frequency was used. The simulation frequency range extended from 300 MHz to 1.5 GHz.

Each of the five bifilar probes with lengths of 14.17 cm, 15.70 cm, 17.20 cm, 18.60 cm, and 20.20 cm was individually optimised in CST using the built-in optimisation library. For every probe, the feed-port position was adjusted until the simulated S11 response in air closely matched the corresponding experimental S11 measurement, ensuring minimal Root Mean Square Error (RMSE) between the real and CST model responses. Table 1 presents the RMSE values of the optimised CST bifilar line geometries compared to their corresponding physical line lengths, S11 parameters magnitude, phase, real and imaginary. The RMSE values illustrate the geometric and electrical alignment between simulated and experimental bifilar probe responses across multiple line configurations.

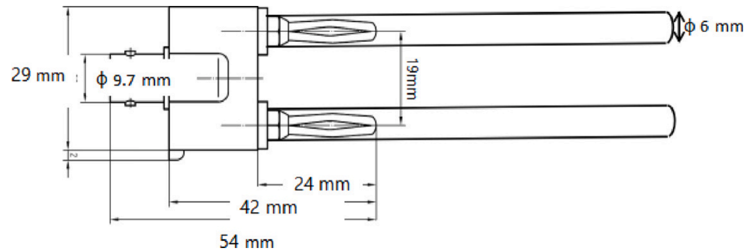

Fig. 3. The configuration of the real bifilar probe.

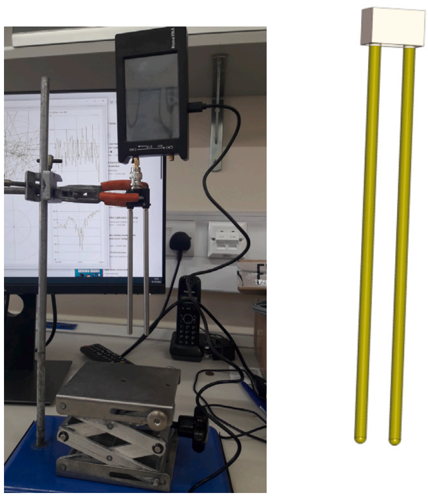

(a) Bifilar line experiment setup in air.

(b) Bifilar line CST Model

Fig. 4. Bifilar line setup in Air.

Table 1
Comparison of measured and simulated S11 for probes with different lengths.

Length (cm)	RMSE mag.	RMSE phase (°)	RMSE real	RMSE imag.
14.19	0.1176	141.6	1.1896	0.8087
15.70	0.3728	101.5	1.1940	0.7929
17.20	0.1150	146.7	1.2352	0.7327
18.60	0.1007	148.8	0.8965	0.6775
20.20	0.1176	141.6	1.1896	0.7625

Reflection coefficient measurements were performed using a commercially available nanoVNA (15 cm × 10 cm × 6 cm), a low-cost vector network analyser offering a dynamic range of 80 dB and typical trace noise of ±0.5 dB. To ensure measurement accuracy, an SOL (Short-Open-Load) calibration protocol was rigorously applied before data acquisition. Fig. 5 illustrates the simulated and experimental S11 magnitude and phase responses for the bifilar probe across the multiple line configurations. Simulations reproduce the modal behaviour; however, they exhibit quantitative discrepancies compared to experimental measurements. The principal resonance frequency diverges between simulation and measurement, with Δf ranging from 30 MHz to 78 MHz. The resonance depth differs slightly, with values of 3.85 dB in the simulation and 3.74 dB in the measurement. Cross-comparison at each resonance reveals a magnitude mismatch of approximately 2.5 to 2.8 dB. Over the frequency range of 0.30 to 1.50 GHz, the band-averaged errors are $\text{RMSE}_{|S11|}$ = 1.26 dB (NRMSE 37.3%) and $\text{RMSE}_{\text{phase}}$ = 123.6° (NRMSE 68.6%). These deviations are attributed to fabrication tolerances, simplified open-end modelling, limited connector de-embedding, and assumptions regarding material properties. This validates simulation methodology and confirms the geometric and electrical fidelity of the bifilar probe design, particularly in preserving impedance characteristics and minimising parasitic effects.

3.2. Simulation data validation of the inversion model

The primary output from the CST simulations of the multilength bifilar probes is the $S11$ parameter, simulated across the frequency range, is then fed into the developed MATLAB inversion code for further processing.

As part of the validation procedure, the algorithm is first tested using air, distilled water, and standard liquids to fine-tune its internal parameters. In Section 3.2.1, the optimised algorithm to achieve the best fit of the $S11$ parameters for air and distilled water is presented. This process allows refinement of key model settings, such as the load impedance Z_L and the position of the discrete port within the probe head, to ensure the best fit with the analytical model.

To ensure the robustness of the approach, the validation is carried out in two stages. First, the simulated S_{11} data is compared with predictions from the analytical model to confirm consistency. Once validated, the algorithm is applied to extract Debye dispersion parameters for the MUT. In Section 3.2.2, the fine-tuned bifilar probe model is used in conjunction with the inversion method and validated against literature-reported permittivity values for standard liquids.

This stepwise validation ensures that the residuals (cost function values) decrease consistently during optimisation. If residuals do not improve as expected, adjustments are made to the Genetic Algorithm (GA) parameters — such as PopulationSize and MaxGenerations — to enhance performance and convergence.

3.2.1. Validation of the simulated reflection coefficient against analytical model

The CST multi-length bifilar probe model was simulated in air ($\varepsilon_r \approx 1$) and distilled water ($\varepsilon_r \approx 80$) to optimise the model for the best agreement between the simulated reflection coefficient (S_{11}) and those obtained from the analytical model (presented in Section 2). This comparison was conducted across five probe lengths to identify the configuration that provides the best fit based on the defined fitness function and Z_L was found to be equal to 10^6 Ω. Fig. 6 presents the simulated ($S11$) responses for both air and distilled water. The shape of the ($S11$) curves reveal distinct frequency-dependent behaviour: for distilled water, the curves show deeper notches and noticeable resonance shifts due to its high permittivity, whereas in air, the response is with minimal oscillations across the frequency range. These differences clearly distinguish between the two materials and confirm the probe's sensitivity to dielectric property variations. The discrepancy between CST simulation and model results originates from specific model assumptions, including the use of an ideal open-ended probe, transverse electromagnetic (TEM) propagation, and simplified loss modelling. Additional errors stem from neglected radiation at the probe tip, incomplete representation of frequency-dependent loss mechanisms, and the assumption of a uniform field distribution across the probe cross-section.

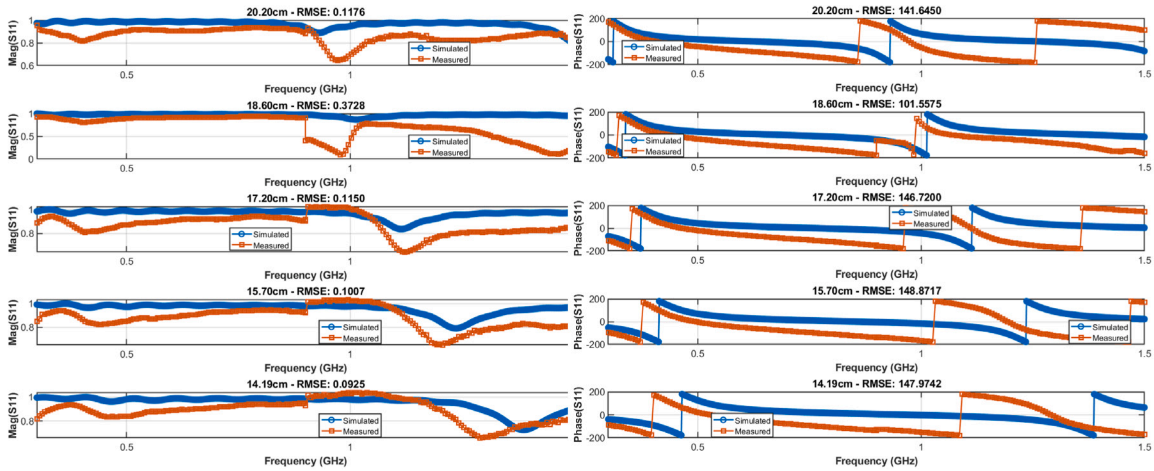

(a) S11 Linear Magnitude (b) S11 Phase

Fig. 5. Comparative analysis of S11 Parameters: CST Simulated vs. Prototype Bifilar Line of different lengths.

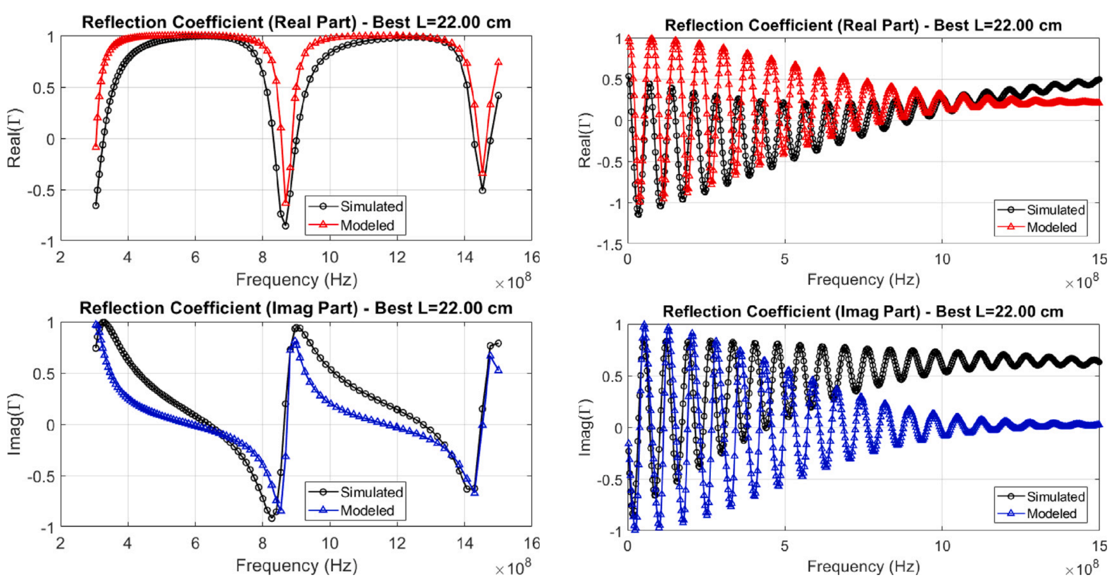

(a) MUT Air (b) MUT Distilled Water

Fig. 6. Reflection coefficient validation against analytical model.

The best fitted $S11$ parameters were used to extract Debye parameters for air ($\epsilon_\infty = 1.18$, $\epsilon_{=}1.37$, $\tau = 8.1 \times 10^{-12}$ (ps), and $\sigma = 1 \times 10^{-7}$ (S/m)) and water($\epsilon_\infty = 4$, $\epsilon_{=}80$, $\tau = 9 \times 10^{-12}$ (ps), and $\sigma = 1 \times 10^{-6}$ (S/m)). The comparison with literature data reported in [24] showed good agreement. For both investigated materials, air and water, the inversion code retrieved the same Debye model parameters across all lengths, respectively. However, the final Debye parameters were extracted based on the minimum cost value among the varying lengths, ensuring the most accurate value.

3.2.2. Simulation validation using standards liquids

Three standard liquids — methanol, ethanol, and propanol-2 — were used as MUT in the CST bifilar line simulations. In each simulation, the section of the bifilar line beneath the top head was fully immersed in the MUT.

The complex permittivity of these materials was measured using a commercially available slim-form probe from Keysight Technologies over a frequency range of 300 MHz to 1.5 GHz, with measurements taken at 101 frequency points. The Keysight 85070E dielectric probe kit was connected to a Rohde & Schwarz ZVA50 vector network analyser (VNA) for data acquisition. This data was fitted to the Debye model parameters for comparison.

The measured complex permittivity values of these materials were imported into the CST material library and assigned to each simulation case. A separate simulation was conducted for each material, with the S11 parameter extracted individually for each length, which was swept parametrically. The S11 parameters for each individual length (14.19, 15.7, 17.2, 18.6, and 20.2 cm) were saved as text files, storing both real and imaginary parts as a function of frequency. These data sets were then imported into the inversion algorithm to retrieve the permittivity of the MUT.

Table 2 compares the extracted Debye model parameters from the multi-length CST simulated model to the literature values for standard liquids and the fitted Slim form measurements data, along with their corresponding RMSE values. RMSE1 and RMSE2 represent the root mean square error (RMSE) values used to evaluate accuracy. RMSE1 quantifies the difference between the complex permittivity extracted from the simulated data Debye model parameters and the literature

Table 2
Retrieved permittivity from the multi-length bifilar CST simulation model, Literature data, and RMSE.

Material	Parameter	Simulations	Literature	RMSE1	Slim probe	RMSE2
Methanol	ϵ_∞	2.0	2-2.2	0.5	7.3321	0.9948
	ϵ_s	33.5	32–33		34.8927	
	τ (ps)	100	50–55		60.15	
	σ (S/m)	10^{-6}	$10^{-6} - 10^{-7}$		9.9×10^{-7}	
Ethanol	ϵ_∞	3.0	4-4.3	6.7	4.8	6.4
	ϵ_s	25.0	24–25		26.77	
	τ (ps)	100	90–100		192.8	
	σ (S/m)	10^{-6}	$10^{-6} - 10^{-7}$		9.9×10^{-7}	
2-Propanol	ϵ_∞	4.0	3.5–4	2.4	2	6.9
	ϵ_s	19.0	19–20		16.33	
	τ (ps)	200	150–200		341.7	
	σ (S/m)	10^{-6}	$10^{-6} - 10^{-7}$		10^{-7}	

Debye model parameters, while RMSE2 measures the difference between the complex permittivity extracted from the simulated data and the complex permittivity obtained using the fitted Slim Form probe data. These metrics provide insight into the accuracy of the inversion algorithm and the reliability of the extracted Debye model parameters, ensuring their consistency and validity.

4. Implementation of the inversion model

The measurements using the bifilar multilength probes were performed using a commercially available miniaturised VNA (m-VNA) over a frequency range of 300 MHz to 1.5 GHz, with 101 frequency points. The m-VNA was directly connected to the bifilar line of the top head and the rods were fully immersed in the MUT. All measurements used a one-port OSL calibration at the SMA feed to set the reference plane at the probe input; the connector–probe transition was modelled and tuned to an air reference to align simulations with experiment, discussed in Section 3. Each acquisition employs five distinct probe lengths with identical material and setup, allowing the spread of retrieved parameters across lengths to serve as an internal repeatability check. If the dispersion meets the defined acceptance criterion, characterised by low spread and absence of outlier lengths, additional triplicate remeasurements for the same material and conditions are unnecessary. The diversity in probe lengths provides sufficient redundancy.

Five different MUTs, listed in Table 3, whose relative complex permittivities were previously measured using the slim-form probe and fitted to Debye model parameters, were used to experimentally validate the multi-length bifilar probe permittivity measurement inversion method (see Fig. 7).

Table 3 presents the retrieved Debye model parameters for the relative complex permittivity of the bifilar prototype. These results are compared to the Debye parameters for the same materials as measured with the slim-form probe. For each candidate probe length L_k, a set of single-pole Debye parameters $\theta = \{\varepsilon_s, \varepsilon_\infty, \tau, \sigma\}$ is obtained using GA by minimising the frequency-domain misfit between the measured and modelled one-port responses. The model calculates $S_{11}^{\text{mod}}(f; \theta_k, L_k)$ using the transmission-line model representation. To enhance clarity, the numerical tables are supplemented with bar graph summaries. Figs. 8 to 12 present grouped bars for the parameters ε_∞, ε_s, τ, and σ, comparing Bifilar probe and Slim-probe measurements. The parameter σ is displayed on a logarithmic scale to accommodate its wide range of values. The tables are included for precise numerical reference.

The root mean square errors (RMSEs) between the complex permittivity estimates and the reference dataset are minimal in absolute value and remain insignificant compared to the variability observed across frequency bands in ε (permittivity), presented in Table 3.

Additionally, the multi-length bifilar system was used to characterise the relative complex permittivity of Bajjad soil and a commercially available soil. For each soil and each probe length L_k, the inversion yields a Debye parameter set $\varepsilon_s, \varepsilon_\infty, \tau, \sigma_k$. Table 4 presents averages of these parameters across all probe lengths: $\varepsilon_s, \varepsilon_\infty, \tau$, and σ. Bajjād soil demonstrates higher values of ε_s, σ, and ε_∞ compared to the commercial reference soil. Increased ε_s and σ are indicative of greater moisture or ionic content and a larger bound-water fraction. A longer τ reflects slower dipolar relaxation, which corresponds to a

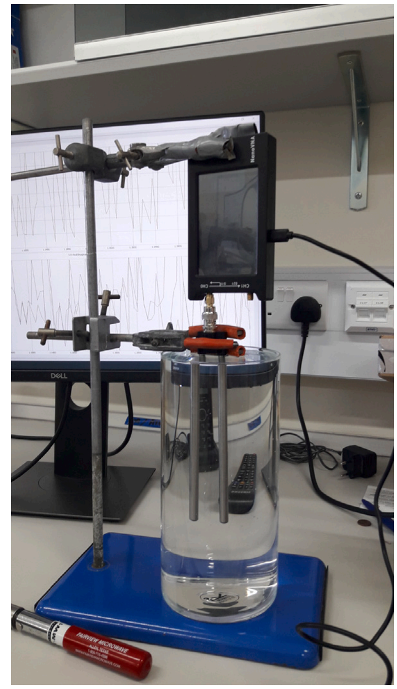

Fig. 7. Experiment Set-up.

Table 3
Comparison of Debye parameters: Simulation vs. standard data sheet.

Material	Parameter	Measurements	Slim probe	RMSE
2-Propanol	ϵ_∞	7.81	2	6.5
	ϵ_s	19.04	16.33	
	τ (ps)	679.00	341.7	
	σ (S/m)	10^{-7}	10^{-7}	
Ethanol	ϵ_∞	4.35	4.8	2.2
	ϵ_s	25.04	26.77	
	τ (ps)	150	192.8	
	σ (S/m)	10^{-7}	9.9×10^{-7}	
Methanol	ϵ_∞	5.88	7.3321	5.4
	ϵ_s	33.50	34.9	
	τ (ps)	80.30	60.15	
	σ (S/m)	10^{-6}	9.9×10^{-7}	
Olive Oil	ϵ_∞	2.25	2.47	0.2
	ϵ_s	2.90	3.25	
	τ (ps)	433.00	810	
	σ (S/m)	10^{-7}	10^{-7}	
Sunflower Oil	ϵ_∞	3.0	3.0	0.44
	ϵ_s	3.9	3.5	
	τ (ps)	9.20	1.00	
	σ (S/m)	10^{-7}	10^{-7}	
Deionised Water	ϵ_∞	4.00	4.20	1.9
	ϵ_s	78.50	80.10	
	τ (ps)	8.20	7.3	
	σ (S/m)	0.0002	10^{-7}	
Air	ϵ_∞	1.2	1	0.6
	ϵ_s	1.6	1	
	τ (ps)	0.7	1	
	σ (S/m)	10^{-7}	10^{-7}	

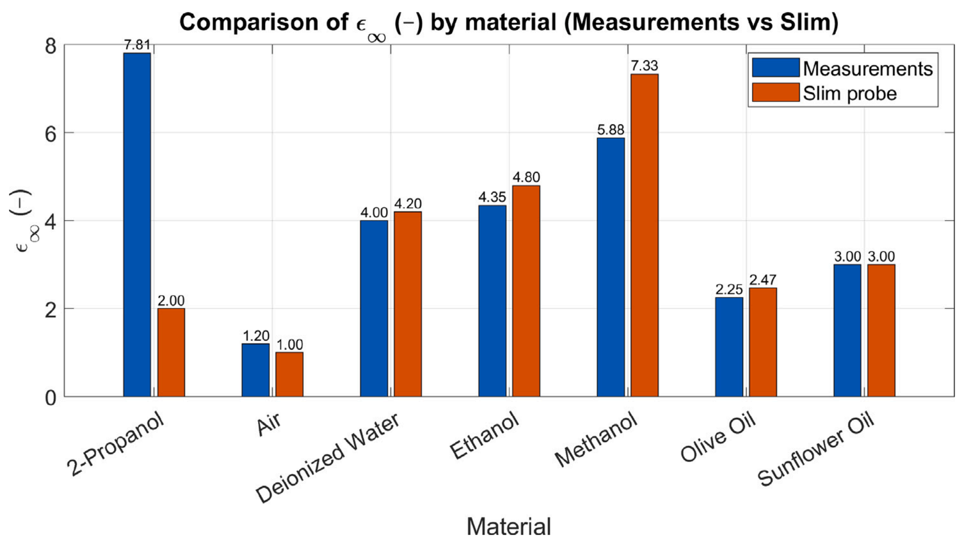

Fig. 8. Comparison of retrieved Debye parameter ε_∞ by material for our method vs. the commercial slim-form probe.

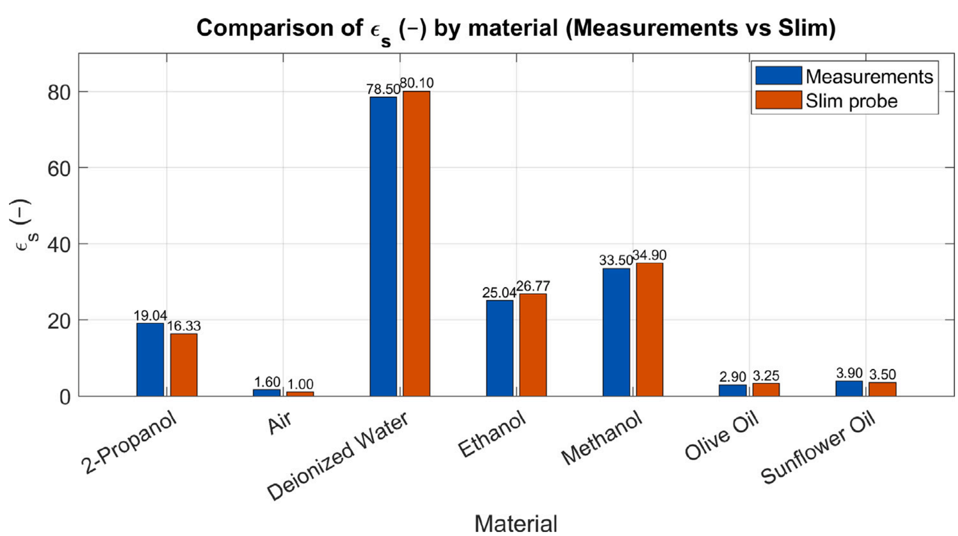

Fig. 9. Comparison of retrieved Debye parameter ε_s by material for our method vs. the commercial slim-form probe.

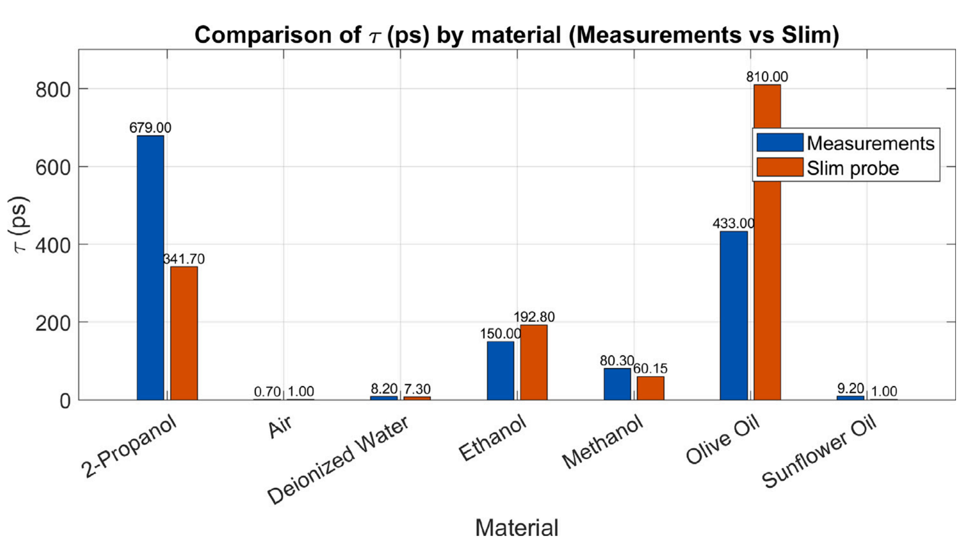

Fig. 10. Comparison of retrieved Debye parameter τ by material for our method vs. the commercial slim-form probe.

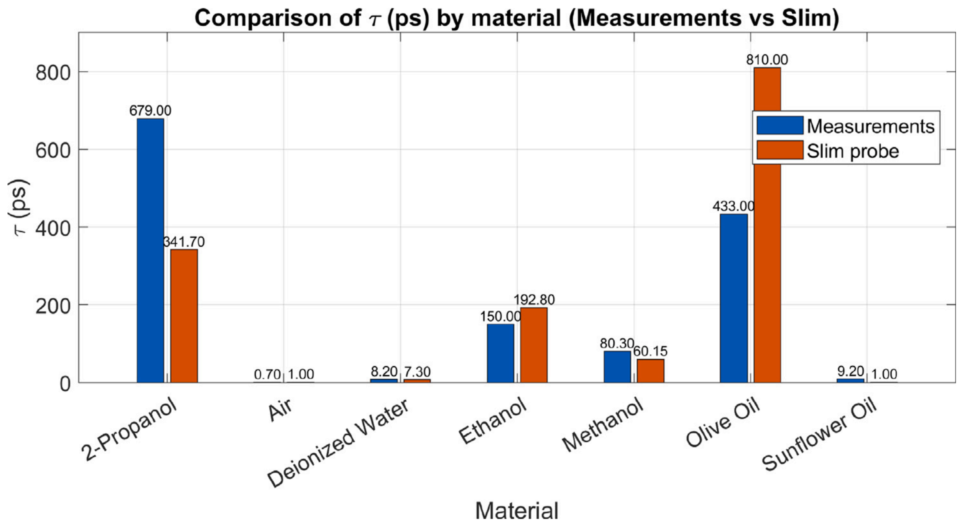

Fig. 11. Comparison of retrieved Debye parameter τ by material for our method vs. the commercial slim-form probe.

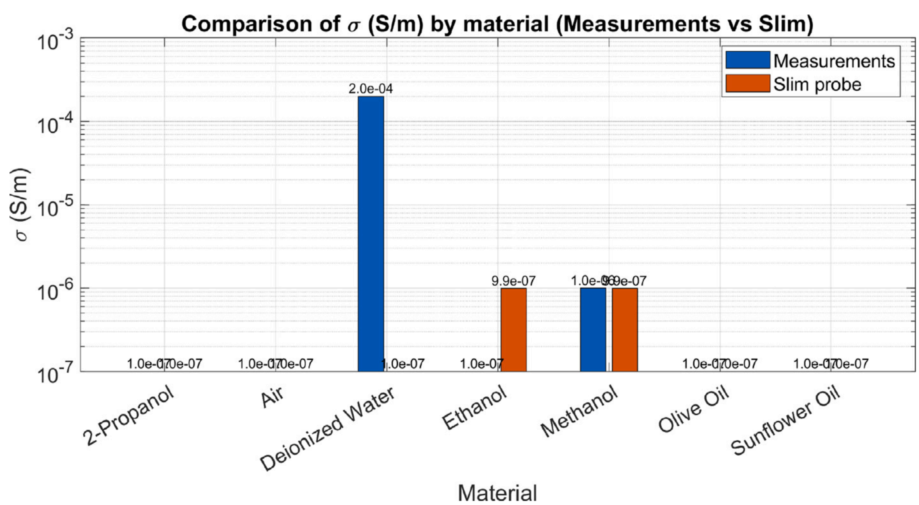

Fig. 12. Comparison of retrieved Debye parameter σ by material for our method vs. the commercial slim-form probe.

Table 4
Comparison of Debye parameters for two soil samples (Two Trials).

Soil Sample	ϵ_∞	ϵ_s	τ (s)	σ (S/m)
Trial 1 (Bajjad)	2.3	3.4	8.5×10^{-10}	8.9×10^{-6}
Trial 2 (Bajjad)	2.4	3.4	8.9×10^{-10}	8.5×10^{-6}
Trial 1 (Commercial Soil)	2.1	3.2	0.6×10^{-12}	8×10^{-6}

higher proportion of bound water. In contrast, a shorter τ means greater water mobility.

The reflection coefficient of Bajjad soil was measured twice to assess the repeatability and consistency of the results. The measurement protocol for bifilar multi-length probes requires sequential insertion for each length. Because the soil is prone to movement and the formation of air gaps, the measurements were repeated twice and designated as trial 1 and trial 2, shown in Table 4. The two independent measurements of Bajjād soil produce statistically consistent parameters. The run-to-run differences are within 0% for ε_s, 0.2 for ε_∞, 0.4×10^{-10} for τ, and $0.4 \times 10^{-6}$for σ. These values are similar to the dispersion observed across different sample lengths, which suggests that instrument noise and minor placement variability are the primary sources of variation rather than systematic drift.

.

5. Conclusion

This study presented a novel bifilar probe methodology for accurately measuring the dielectric properties of materials, particularly liquids and semi-solids. The proposed multi-length bifilar structure demonstrated high precision in characterising complex permittivity over a frequency range of 300 MHz to 1.5 GHz. By leveraging a hybrid inversion algorithm, combining Genetic Algorithms (GA) and Sequential Quadratic Programming (SQP), the methodology successfully extracted Debye model parameters from both simulated and experimental data.

The validation process included comparisons with literature values and measurements obtained using a commercial slim-form probe, with RMSE values confirming the accuracy of the inversion model. Additionally, the system was applied to soil characterisation, demonstrating its applicability to real-world scenarios such as environmental monitoring and agricultural sensing.

Overall, the results validate the efficacy and repeatability of the proposed method, offering a cost-effective, customisable, and replicable approach for dielectric property measurement. The multi-length bifilar system extends the capabilities of conventional techniques, making it a valuable tool for various applications in biomedical applications, material science, sensing technologies, and geophysical exploration.

CRediT authorship contribution statement

Iman Farhat: Conceptualization, Methodology, Software, Validation, Writing – original draft. **Raffaele Persico:** Conceptualization, Methodology, Software, Reviewing. **Justin Stellini:** Data curation, Investigation. **Andrea Cataldo:** Model assembly. **Julian Bonello:** Visualization. **Lourdes Farrugia:** Supervision, Reviewing.

Declaration of competing interest

The authors declare that they have no known competing financial interests or personal relationships that could have appeared to influence the work reported in this paper.

Acknowledgment

This research was funded by the Energy and Water Agency Malta within the framework of the National Strategy for Research in the Energy and Water Sectors.

Data availability

Data will be made available on request.

References

[1] Raffaele Persico, Andrea Cataldo, Egidio De Benedetto, Chapter 3 - time-domain reflectometry: Current uses and new possibilities, in: Raffaele Persico, Salvatore Piro, Neil Linford (Eds.), Innovation in Near-Surface Geophysics, Elsevier, 2019, pp. 59–96.
[2] D.A. Robinson, S.B. Jones, J.M. Wraith, D. Or, S.P. Friedman, A review of advances in dielectric and electrical conductivity measurement in soils using time domain reflectometry, Vadose Zone J. 2 (4) (2003) 444–475.
[3] G.C. Topp, J.L. Davis, A.P. Annan, Electromagnetic determination of soil water content: Measurements in coaxial transmission lines, Water Resour. Res. 16 (3) (1980) 574–582.
[4] Scott B. Jones, Jon M. Wraith, Dani Or, Time domain reflectometry measurement principles and applications, Hydrol. Process. 16 (1) (2002) 141–153.
[5] J.A. Huisman, S.S. Hubbard, J.D. Redman, A.P. Annan, Measuring soil water content with ground penetrating radar, Vadose Zone J. 2 (4) (2003) 476–491.
[6] Luigi Ragni, Annachiara Berardinelli, Chiara Cevoli, Enrico Valli, Assessment of the water content in extra virgin olive oils by time domain reflectometry (TDR) and partial least squares (PLS) regression methods, J. Food Eng. 111 (1) (2012) 66–72.
[7] A. Cataldo, M. Vallone, L. Tarricone, G. Cannazza, M. Cipressa, TDR moisture estimation for granular materials: An application in agro-food industrial monitoring, IEEE Trans. Instrum. Meas. 58 (8) (2009) 2597–2605.
[8] M. Kent, W. Meyer, Determination of moisture content in oil by time domain reflectometry, J. Food Eng. 47 (2) (2001) 129–137.
[9] David M. Pozar, Microwave engineering, John Wiley & Sons, 2011.
[10] Raffaele Persico, Massimiliano Pieraccini, Measurement of dielectric and magnetic properties of materials by means of a TDR probe: a preliminary theoretical investigation in the frequency domain, Near Surf. Geophys. 16 (2) (2018) 118–126.
[11] Wesley Beccaro, Daniel Rochinha, Henrique Peres, Fatima Correra, Analysis of different probe geometries for ethanol fuel qualification using time-domain reflectometry, Prog. Electromagn. Res. Lett. 61 (2016) 105–109.
[12] Wojciech Skierucha, Andrzej Wilczek, Marek Horyński, Andrzej Sumorek, Determination of electromechanical properties of dusts obtained from cereal grain, Trans. the ASABE (American Soc. Agric. Biological Engineers) 51 (2008) 177–184.
[13] Raffaele Persico, Iman Farhat, Lourdes Farrugia, Charles Sammut, A numerical investigation of the dispersion law of materials by means of multi-length TDR data, Remote. Sens. 14 (9) (2022).
[14] Andrea Cataldo, Iman Farhat, Lourdes Farrugia, Raffaele Persico, Raissa Schiavoni, A method for extracting debye parameters as a tool for monitoring watered and contaminated soils, Sensors 22 (20) (2022).
[15] Dassault Systèmes, CST Studio Suite, 2023, Computer Simulation Technology (CST), 3D Electromagnetic Simulation Software.
[16] S.J. Zegelin, I. White, D.R. Jenkins, An improved field method for measuring water content of a soil at radio frequencies, J. Hydrol. 102 (1–4) (1989) 367–383.
[17] B.J.J. van der Vlist, A. Dolstra, G. van der Zwan, Accurate and efficient computation of the dielectric permittivity of water from microwave to millimeter-wave frequencies, IEEE Trans. Microw. Theory Tech. 51 (5) (2003) 1519–1526.
[18] N. Wagner, K. Emmerich, F. Bonitz, K. Kupfer, Evaluation of TDR and capacitance techniques for soil moisture measurement, IEEE Trans. Geosci. Remote Sens. 49 (3) (2011) 898–911.
[19] C.L. Jones, M.L. Stone, Electromagnetic sensing methods for nondestructive evaluation of food materials, Instrum. Meas. Technol. Conf. (2005) 1829–1834.
[20] S. Ramo, J. Whinnery, T. Van Duzer, Fields and Waves in Communication Electronics, John Wiley & Sons, 1965.
[21] E.I. Green, F.A. Leibe, H.E. Curtis, The proportioning of shielded circuits for minimum high-frequency attenuation, Bell Syst. Tech. J. 15 (2) (1936) 248–283.
[22] M.N.O. Sadiku, Elements of electromagnetics, Oxford University Press, 2006.
[23] Inc. The MathWorks, MATLAB, 2024.
[24] Johan Huisman, W. Bouten, Jasper Vrugt, Ty Ferré, Accuracy of frequency domain analysis scenarios for the determination of complex dielectric permittivity, Water Resour. Res. 40 (2004).